Nascent RNA sequencing defines dynamic aryl hydrocarbon receptor signaling responses to wood smoke particles

Arnav Gupta[1,2], Sarah K. Sasse[2], Lynn Sanford[3], Margaret A. Gruca[3], Robin D. Dowell[3,4,5], and Anthony N. Gerber*[1, 2,6]

[1]Department of Medicine, University of Colorado, Aurora, CO, 80045, USA.

[2]Department of Medicine, National Jewish Health, Denver, CO, 80206, USA.

[3]BioFrontiers Institute, University of Colorado, Boulder, CO, 80309, USA.

[4]Molecular, Cellular and Developmental Biology, University of Colorado, Boulder, CO 80309, USA.

[5]Computer Science, University of Colorado, Boulder, CO, 80309, USA.

[6]Department of Immunology and Genomic Medicine, National Jewish Health, Denver, CO, 80206, USA.

Running title: Wood smoke transiently activates the aryl hydrocarbon receptor

*To whom correspondence should be addressed:

Dr. Anthony N. Gerber, Department of Medicine, National Jewish Health, Room K729, 1400 Jackson St, Denver, CO, 80206, USA, Tel.: 303-270-2783, E-mail: gerbera@njhealth.org

Abstract

Transcriptional responses to wildfire smoke, an increasingly important cause of human morbidity, are poorly understood. Here, using a combination of precision nuclear run-on sequencing (PRO-seq) and the assay for transposase-accessible chromatin using sequencing (ATAC-seq), we identify rapid and dynamic changes in transcription and chromatin structure in Beas-2B airway epithelial cells after exposure to wood smoke particles (WSP). By comparing 30 and 120 minutes of WSP exposure, we defined three distinct temporal patterns of transcriptional induction and chromatin responses to WSP. Whereas transcription of canonical targets of the aryl hydrocarbon receptor (AHR), such as *CYP1A1* and *AHRR*, was robustly increased after 30 minutes of WSP exposure, transcription of these genes and associated enhancers returned to near baseline at 120 minutes. ChIP-qPCR assays and AHR knockdown confirmed a role for AHR in regulating these transcriptional responses, and we applied bioinformatics approaches to identify novel AHR-regulated pathways and targets including the DNA methyltransferase, *DNMT3L,* and its interacting factor, *SPOCD1*. Our analysis also defined a role for NFkB as a primary transcriptional effector of WSP-induced changes in gene expression. The kinetics of AHR- and NFkB-regulated responses to WSP were distinguishable based on the timing of both transcriptional responses and chromatin remodeling, with induction of several cytokines implicated in maintaining the NFkB response. In aggregate, our data establish a direct and primary role for AHR in mediating airway epithelial responses to WSP and identify crosstalk between AHR and NFkB signaling in controlling pro-inflammatory gene expression.

Introduction

As a consequence of climate change, wildfires are increasing in size and prevalence worldwide, resulting in expanded impacts of wildfire air pollution on heavily populated areas (1). This was dramatically exemplified by the 2020 wildfire season in western North America in which large urban areas ranging from Los Angeles, CA to Denver, CO to Vancouver B.C. experienced high levels of wildfire-associated particulate matter (PM) pollution over periods extending for weeks (2). Such wildfire PM pollution has been associated with a variety of health effects including respiratory symptoms, inflammation, exacerbations and morbidity (3-5). Acute health consequences of PM pollution disproportionately impact the young, the elderly, and those with preexisting health conditions, whereas long-term exposure to high levels of PM is itself a risk factor for developing lung disease (6). The mechanisms responsible for acute and chronic health effects of wildfire pollution are not well understood.

Pollution and resultant health effects that arise from wildfires cannot be directly controlled through traditional regulatory constraints directed at other sources of toxic air pollution (e.g. vehicle emissions and large stationary sources). Instead, general air quality-based warnings and cautions (7), which are issued on a regional basis when pollution exceeds standard PM thresholds (8-11), are the primary measure used to mitigate health effects of wildfire smoke. Although these daily warnings are useful for alerting impacted populations of potential health risks, they lack granular information regarding toxicity (7,12,13). This can vary considerably based on the underlying characteristics of the burning biomass, the potential for combustion of manufactured materials when wildfires extend into developed regions, and the distance of an impacted area from the wildfire. These warnings are also directed, based on predicted impact of specific PM levels, to relatively large population subsets such as “the very young” or those with “heart disease”, and thus fail to accurately advise on individual health risk (9). Furthermore, during prolonged periods of high PM levels, these warnings can serve to limit otherwise beneficial outdoor exercise and activities that improve both physical and mental health. Thus, a better understanding of wildfire-specific respiratory toxicity is necessary to optimize and provide personalized guidance to exposed populations during wildfire events and also to identify preventive therapeutics that mitigate risk.

Wood smoke particles (WSP) derived from controlled combustion of wood have been previously used as a model to study wildfire smoke exposure (14-16). These WSP are composed of a heterogeneous mix of

compounds including fine and coarse particulate matter, heavy metals, poly-aromatic hydrocarbons (PAHs) and volatile organic compounds (VOCs), which depend on the source of combustible material, similar to bona fide wildfire pollution (15). Experimental WSP inhalation in healthy individuals recruits inflammatory cells, stimulates oxidative damage and impairs immune responses to viral infections (17-19). WSP exposure in cell culture models causes cytotoxicity, genotoxicity, cellular stress, formation of reactive oxygen species (ROS), and increased expression of pro-inflammatory cytokines (16,20,21). However, the molecular and transcriptional control of these effects has not been fully elucidated.

Several pathways have been identified as regulating gene expression responses to other sources of air pollution, such as diesel exhaust particles (DEP), in cell types of high relevance to wildfire toxicity (22-24). For example, transcriptional effects of DEP exposure in the lung have been linked to activation of the inflammasome, NFkB, and aryl hydrocarbon receptor (AHR) signaling (25-28). The AHR is a bHLH-Pas domain transcription factor which, upon ligand binding, translocates to the nucleus and controls gene expression through binding to xenobiotic response elements (XREs) found in regulatory regions of target genes (29-32). AHR functions as a heterodimer with ARNT and directly induces expression of canonical antioxidant and detoxification genes such as the Cytochrome P450 family (31). AHR strongly induces the expression of AHRR (33,34), which forms heterodimers with ARNT, thereby repressing AHR transcriptional activity in a potent negative feedback system. Numerous ligands have been identified for AHR, including the prototypical ligand 2,3,7,8 tetrachlorodibenzo-p-dioxin (TCDD) (31), PAH compounds found in products of combustion (35), as well as several endogenous ligands (36). Although comparatively little is known about how different AHR ligands alter AHR transcriptional specificity and response kinetics, induction of AHR signaling in response to toxins such as TCDD is generally regarded as deleterious (37), whereas endogenous AHR ligands are implicated in promoting beneficial effects on the immune system (32,38). Whether WSP directly activates AHR signaling has not been definitively established.

In this study, to define the mechanisms underlying the effects of WSP on airway epithelial gene expression, we exposed Beas-2B cells, a cultured human airway epithelial cell model, to WSP. We assayed genome-wide nascent transcriptional responses and chromatin accessibility changes after 30 and 120 minutes of exposure to WSP. We applied bioinformatics tools to cluster expression and epigenetic responses into distinct

temporal patterns and to identify transcription factors that mediate these effects. We employed ChIP-qPCR and siRNA-mediated gene knockdown to test directly whether AHR and NFkB mediate transcriptional responses to WSP in airway epithelial cells.

Methods

Cell Culture

Beas-2B immortalized human bronchial epithelial cells were obtained from ATCC and cultured in Dulbecco's Modified Eagle Medium (DMEM; Corning) with L-glutamine and 4.5 g/L glucose supplemented with 10% Fetal Bovine Serum (FBS; VWR) and 1% penicillin/streptomycin (Corning). De-identified primary human small airway epithelial cells (< 2 mm diameter; smAECs) were obtained from the National Jewish Health Biobank and plated onto an irradiated NIH/3T3 (ATCC) fibroblast feeder layer in F-medium containing 1 uM Y-27632 (APEX Bio). Upon visible colony formation (~7-10 days), smAECs were removed with 0.25% trypsin (Corning), plated on tissue culture dishes double-coated with Type I bovine collagen solution (Advanced Biomatrix), and grown to confluence in BronchiaLife Epithelial Medium supplemented with the complete LifeFactors Kit from Lifeline Cell Technology. All cells were maintained in 5% CO_2 at 37°C.

Wood Smoke Particle (WSP) Exposure

Wood Smoke Particles (WSP) were generated as described (14) and generously gifted by Dr. Andrew Ghio at the Environmental Protection Agency Laboratory in North Carolina. Particles were dehydrated for transportation and resuspended in PBS. Particles were disaggregated by sonication and sterilized under UV light for 20 minutes prior to addition directly to cell culture media at a concentration of 1 mg/ml for all experiments.

RNA purification and quantitative reverse transcription-PCR (qRT-PCR)

Beas-2B cells or smAECs were grown to confluence in 6-well tissue culture dishes (collagen-coated for smAECs, as described above) and treated with vehicle (PBS) or WSP for 2, 4 or 24 hours. Cells were harvested in TRIzol (Life Technologies) and RNA purified by PureLink RNA Mini Kit (Life Technologies) prior to qRT-PCR, performed with normalization to *RPL19* as previously detailed (39). Sequences of primers used for qRT-PCR analysis are provided in Supporting Table S1.

Precision Run-on Sequencing (PRO-seq)

Beas-2B cells were plated on 3 x 15 cm tissue culture dishes per treatment and grown to confluence, then treated with vehicle (PBS) or WSP for 30 or 120 minutes. Cells were harvested and nuclei prepared as reported previously (39). Aliquots of 10E6 nuclei were subjected to 3-minute nuclear run-on reactions in the presence of Biotin-11-CTP (PerkinElmer) and PRO-seq libraries were constructed in duplicate as described (40). Uniquely indexed libraries were pooled and sequenced on an Illumina NextSeq instrument using 75 bp single-end reads by the BioFrontiers Sequencing Facility at the University of Colorado Boulder.

PRO-seq Computational Analysis

PRO-seq data were processed using a standardized Nextflow pipeline (https://github.com/Dowell-Lab/Nascent-Flow). A complete pipeline report detailing all software programs and versions utilized and a detailed quality control report including trimming, mapping, coverage, and complexity metrics are included in Supporting File S1. TDF coverage files output by the pipeline, normalized by reads per million mapped, were visualized using the Integrative Genomics Viewer (IGV) genome browser (v. 2.8.0). FStitch (v. 1.0) and Tfit (v. 1.0) were used to identify regions with bidirectional transcriptional activity as described (39). Counts were calculated for each sorted BAM file using multiBamCov from the BEDTools suite (v. 2.28.0) and RefSeq:NCBI Reference Sequences for hg38 downloaded from the UCSC genome browser (May 18, 2018). Genes and lncRNAs were then filtered such that only the isoform with the highest number of reads per annotated length was kept, and DESeq2 (v. 1.20.0, Bioconductor release v. 3.7) was used to determine differentially transcribed genes between treatments. Gene clustering was then performed by intersecting differentially transcribed gene lists to form early-peak (upregulated in 30 min WSP vs vehicle and downregulated in 120 min vs 30 min WSP), early-plateau (upregulated in 30 min WSP vs vehicle and up in 120 min WSP vs vehicle) and late (upregulated in 120 min WSP vs vehicle and upregulated in 120 min vs 30 min WSP) temporal clusters. Functional annotation of differentially regulated genes was performed using DAVID v. 6.8 (41). For bidirectional comparisons, all predicted bidirectional Tfit calls were aggregated using mergeBed (argument -d 60) from BEDTools (v. 2.28.0) to generate an annotation file. Counts were then calculated for each sample using multicov (BEDTools v. 2.28.0), and DESeq2 was used to identify differentially transcribed bidirectionals between treatments.

Assay for Transposase Accessible Chromatin using Sequencing (ATAC-seq)

Beas-2B cells were grown to confluence in 6-well tissue culture dishes and treated with vehicle (PBS) or WSP for 30 or 120 minutes. Cells were rinsed and scraped in ice-cold PBS, then ~50K cells from each treatment were pelleted and processed in duplicate for Omni-ATAC-seq using the protocol developed by Corces et al (42). Uniquely indexed libraries were pooled and sequenced on an Illumina NextSeq using 37 bp paired-end reads by the BioFrontiers Sequencing Facility at the University of Colorado Boulder.

ATAC-seq Computational Analysis

ATAC-seq reads were trimmed for adapters, minimum length, and minimum quality using the bbduk tool from the BBMap Suite (v. 38.73) with arguments 'ref=adapters.fa ktrim=r qtrim=10 k=23 mink=11 hdist=1 maq=10 minlen=20'. Quality control was monitored both pre- and post-trim for all samples using FastQC (v. 0.11.8). Trimmed reads were mapped to the human genome (hg38; downloaded from the UCSC genome browser on September 16, 2019, with corresponding hisat2 index files) using hisat2 (v. 2.1.0). Resulting SAM files were converted to sorted BAM files using samtools (v. 1.9) and to bedGraph coverage format using genomeCoverageBed from the BEDTools suite (v. 2.29.2). Read coverage was then normalized to reads per million mapped using a custom python script and files converted to TDF format using igvtools (v. 2.5.3) for visualization in IGV. MACS2 (v. 2.1.4) callpeak with '--SPMR' argument was applied to sorted BAM files for each replicate pair of samples with parameters set to call peaks with $\log_2$ fold change > 1 above baseline with q < 1e-5 as significant. Peaks were then assigned to early-peak, early-plateau, and late temporal clusters based on simple presence/absence criteria within indicated treatment groups, illustrated by Venn diagrams in Figure 4.

Differential Transcription Factor Motif Enrichment

Transcription factor enrichment analysis for both PRO- and ATAC-seq datasets was performed using TFEA (v. 1.0; https://github.com/Dowell-Lab/TFEA; (43)). Sets of consensus regions of interest (ROIs) are first defined for all Tfit-called bidirectionals (for PRO-seq) or all MACS2-called peaks (for ATAC-seq) using the muMerge function of TFEA. TFEA then calculates read coverage for each replicate within each ROI and applies DESeq2 to determine differentially represented ROIs by treatment condition and assign rank as a function of p-value. For each ranked ROI, the FIMO tool (44) from the MEME suite scans the 3 kb sequence surrounding the ROI center (bidirectional origin or ATAC-seq peak summit) for positions of transcription factor consensus motif matches (with p-value cutoff of 10-5), represented by a curated set of position weight matrices (45). Enrichment scores

(E-scores) for each motif are then calculated and corrected for sequence content to reduce known biases associated with local GC enrichment and p-values are determined using Z-scores. Motif displacement distributions (as in Figure 3C) are displayed as heatmaps where the locations of all motif instances within 1500 bps are indicated relative to the site of RNA polymerase loading and initiation (typically the center of the bidirectional). The intensity of color is a normalized fraction of motif instances within that bp range relative to the entire 3k region total number of motifs.

Chromatin Immunoprecipitation (ChIP)-qPCR

Beas-2B cells were grown to confluence in 10 cm tissue culture dishes and treated with vehicle or WSP for 30 or 120 minutes. Cells were crosslinked by adding 16% methanol-free formaldehyde to a final concentration of 1% and incubating for 5 minutes at room temperature, then ChIP-qPCR was then performed as described (46) using 35 cycles of sonication. A mouse monoclonal antibody raised against AHR was purchased from Santa Cruz (sc-133088 X) and used at a concentration of 5 ug/sample. Assays were performed in biologic quadruplicate. ChIP-qPCR primer sequences are listed in Supporting Table S2.

Western Blotting

Western blotting and protein detection were performed using standard protocols (47) in unstimulated Beas-2B cells cultured to confluence in 6-well plates or following siRNA transfection, as detailed below. Primary antibodies purchased from Santa Cruz included anti-AHR (sc-133088X), anti-NFKB p65 (sc-372), and anti-GAPDH (sc-25778). Secondary antibodies were ECL Donkey anti-Rabbit IgG, HRP-linked F(ab')$_2$ fragment (NA9340) and ECL Sheep anti-Mouse IgG, HRP-Linked Whole Ab (NA931), both from GE Healthcare/Amersham.

siRNA-mediated Gene Knockdown

Beas-2B cells were plated in 6-well tissue culture dishes in antibiotic-free medium. Approximately 24 hours later, cells were transfected with ON-TARGETplus siRNA SMARTpools (Horizon/Dharmacon) against human AHR (si-*AHR*; L-004990-00), RELA (si-*RELA*; L-003533-00), or a scrambled control (si-Ctrl; D-001810-10), at a final concentration of 25 nM using Lipofectamine RNAiMAX transfection reagent (Life Technologies) as instructed by the manufacturer. Media was replaced with fresh complete ~18 hours post-transfection, then 24

hours later, cells were treated with vehicle or WSP for 2 hours for qRT-PCR assays or harvested without additional stimulation for verification of knockdown via Western Blotting.

Statistics

Statistical comparisons for qRT-PCR and ChIP-qPCR assays were made by 2-tailed t-test using the Bonferroni correction when appropriate. These analyses were conducted using statistical software embedded in Open Office (Apache OpenOffice v 4.1.7 http://www.openoffice.org/welcome/credits.html).

Data Availability

Raw and processed sequencing data have been submitted to the NCBI Gene Expression Omnibus (GEO; https://www.ncbi.nlm.nih.gov/geo/). The accession number is GSE167372.

Results

WSP exposure causes rapid and temporally dynamic changes in gene transcription

Exposures that model ambient air pollutants have been reported to cause gene expression changes in airway cells, however the transcriptional cascades that control this process have not been fully elucidated. We exposed Beas-2B cells, a transformed human bronchial epithelial cell line, to WSP in submerged culture. We analyzed changes in gene expression after 2, 4 and 24 hours of exposure using qRT-PCR, focusing on previously identified targets of particulate matter in airway cells and NFkB target genes (28,47-49). We observed rapid induction of five candidate exposure-regulated genes (Figure 1A), with peak expression observed after just two hours of treatment. A similar rapid response to WSP was observed in primary human small airway epithelial cells (smAECs) grown in submerged culture (Figure 1B). Thus, airway epithelial cells exhibit prompt and dynamic changes in gene expression in response to WSP.

To explore the earliest transcriptional responses to WSP and determine underlying mechanisms, we conducted nascent transcript analysis of Beas-2B cell responses to WSP using PRO-seq (50). PRO-seq measures gene transcription with high temporal resolution based on RNA polymerase II activity and also allows for quantification of enhancer activity based on bidirectional signatures of enhancer RNA (eRNA) transcription (51,52). To define direct transcriptional responses to WSP and their initial dynamics, we analyzed nascent

transcription after 30- and 120-minute exposure times relative to treatment with vehicle (PBS). We initially

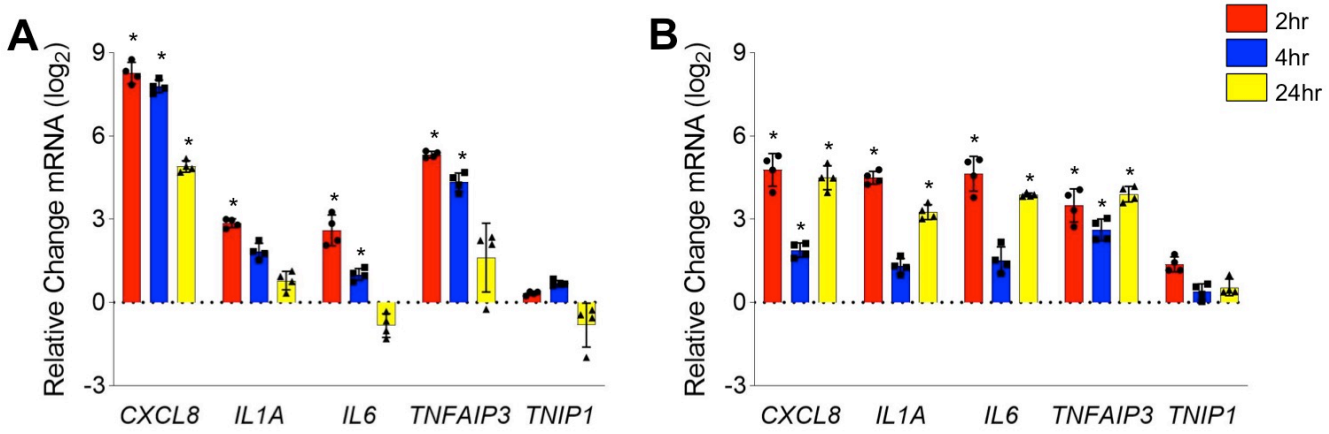

Figure 1. WSP exposure induces inflammatory gene transcription in cultured airway epithelial cells. qRT-PCR analysis of indicated gene expression in (A) Beas-2B cells or (B) smAECs treated with WSP (1 mg/ml) for 2, 4 or 24 hours. Bars represent mean normalized C_T values on a $\log_2$ scale (±SD) relative to vehicle-treated controls (n = 4/group, *$p < 0.05$ vs. vehicle).

focused our analysis on changes in gene transcription in relationship to exposure time. As visualized in volcano plots (Figure 2A), at the 30-minute time point, increased transcription was the dominant response to WSP exposure, with many of these rapidly induced targets exhibiting reduced expression at 120 minutes relative to 30 minutes. We subsequently defined three distinct temporal clusters of transcriptional induction in response to WSP, as indicated by Venn diagrams in Figure 2B and detailed in the Methods, encompassing early-peak, early-plateau, and late clusters of differentially regulated gene transcripts. Complete gene lists for each cluster are presented in Supporting Tables S3-S5, respectively. PRO-seq data were visualized in the Integrative Genomics Viewer (IGV) genome browser (53) and representative data tracks for each temporal cluster are shown in Figure 2B.

Next, to determine whether the different clusters represent distinct biologic processes regulated by WSP as a function of time, we performed functional annotation of the clusters using DAVID (41). Although there were annotation differences between all three clusters (Figure 2C; complete output for each cluster is listed in Supporting Tables S6-S8), comparison of the late cluster to the early-peak and early-plateau annotations showed significant divergence in enriched pathways. In addition, annotation of the early-peak cluster identified

enrichment of AHR-related pathways including Cytochrome P450 metabolism (p = 6.438e-5) and PAS domain-

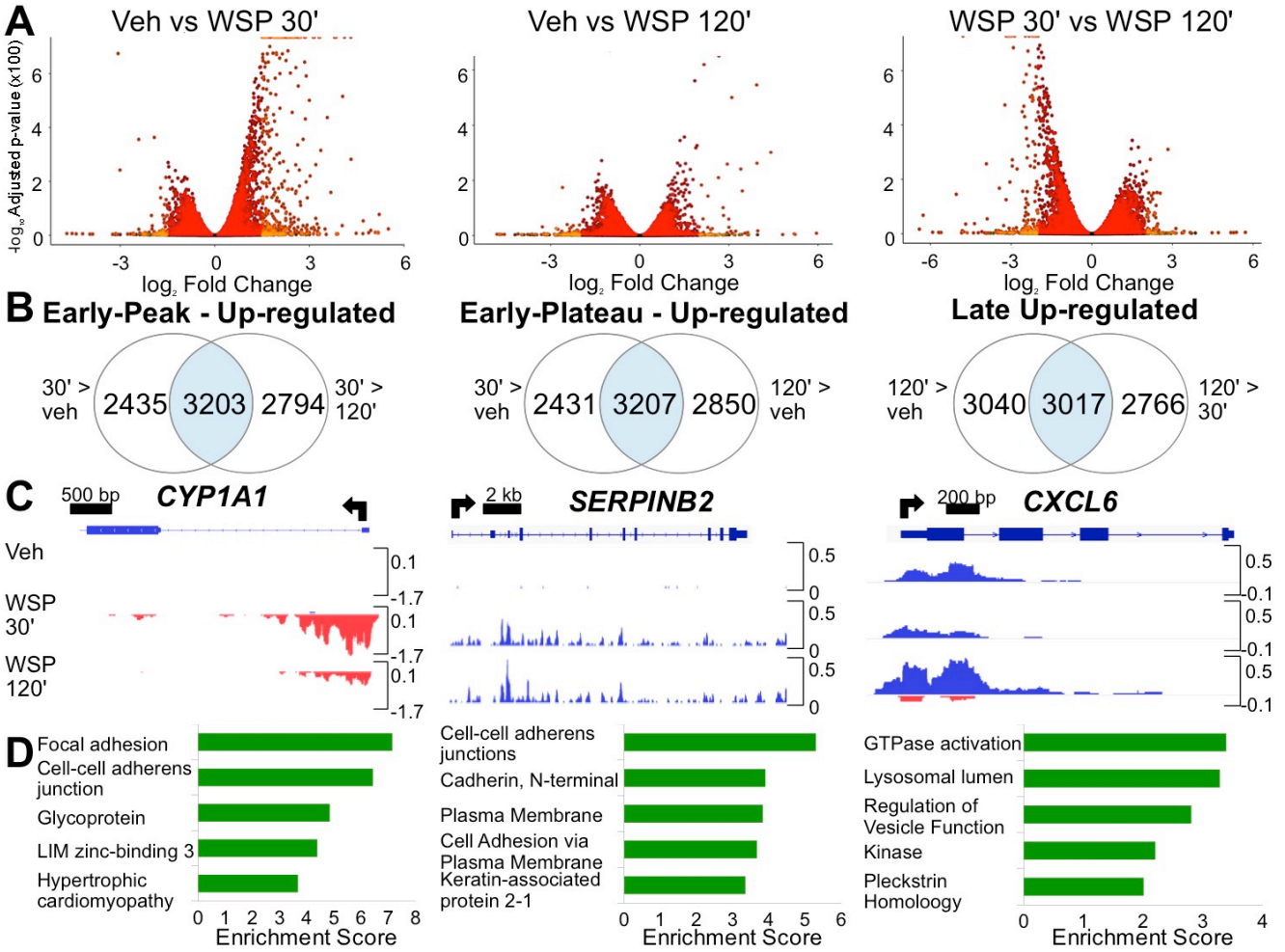

Figure 2. PRO-seq reveals distinct temporal patterns of rapid and transient transcriptional responses to WSP exposure. (A) Volcano plots illustrate differentially regulated nascent transcripts in Beas-2B cells treated with vehicle or WSP for 30 or 120 minutes and compared as indicated. Each point represents one gene, with light orange indicating $p_{adj} < 0.05$ and $\log_2$ fold change > 1, and red signifying differences not meeting both these criteria. Points justified to top of y-axis represent genes with an infinitesimally small p_{adj} that rounds to 0. (B) Criteria used to cluster genes by temporal kinetics of transcriptional induction by WSP and Venn diagrams showing number of differentially regulated transcripts (based on $p_{adj} < 0.05$) meeting these criteria. (C) Representative examples of each temporal cluster characterized in (B) shown as PRO-seq tracks visualized in the Integrative Genomics Viewer (IGV) genome browser based on counts per million mapped reads (vertical scales). Positive (blue) indicates reads annotated to the sense strand while negative (red) peaks reflect reads annotated to the antisense strand. The TSS and direction of transcription are indicated by arrows at the top of each panel. (D) Bar graphs display top 5 most significantly enriched functional annotation terms output by DAVID Functional Annotation Clustering applied to each set of WSP-induced transcripts characterized in (B).

containing transcription factors (p = 3.399e-5). Functional annotation of early-plateau cluster genes also identified enrichment of PAS domain-containing transcription factors (p = 7.424e-4) and NFkB signaling pathways (p = 9.775e-3). In aggregate, our analysis of nascent transcription indicates that WSP exposure causes

a rapid remodeling of airway epithelial gene expression and associated cellular processes. These changes are temporally dynamic, and ontology analysis implicates AHR and NFkB as potential transcriptional mediators of early effects of WSP exposure on transcription.

Enhancer RNA (eRNA) transcription is regulated by WSP

To further study mechanisms underlying regulation of gene expression by WSP, we next analyzed changes in enhancer expression by utilizing Tfit to identify bidirectional signatures of RNA Polymerase II activity associated with nascent eRNA and promoter transcription (52). We then used DEseq2 to determine differential expression of these bidirectional transcripts following vehicle or WSP exposure at both time points. Through this analysis we defined clusters of bidirectional transcription regulation in response to WSP analogous to the clusters observed for gene transcription (Figure 3A). Examples of these distinct bidirectional transcript response patterns to WSP as visualized in IGV are shown in Figure 3B. Complete lists of differentially transcribed bidirectionals from early-peak, early-plateau, and late temporal clusters, as well as hg38 genomic coordinates for all identified bidirectional transcripts, are provided in Supporting Tables S9-S12, respectively. Taken together, these data indicate that dynamic changes in airway epithelial cell gene expression in response to WSP are associated with rapid changes in enhancer activity.

Dynamic changes in enhancer activity generally result from differential transcription factor binding within the enhancer. Therefore, to identify transcription factors that control the primary response to WSP exposure, we interrogated enhancer regions whose activity, based on PRO-seq signatures, changed dynamically in response to WSP exposure. To accomplish this, we identified the origin of bidirectional transcription and applied the Transcription Factor Enrichment Analysis (TFEA) tool to these regions to identify differential motif enrichment (DME) for specific transcription factors (43). TFEA quantifies the degree of co-localization of transcription factor motif instances within the center of specific genomic regions, which in this case are sites of bidirectional transcription. We therefore compared changes in enrichment (E-) scores between vehicle and 30 minutes, 30 minutes and 120 minutes, and vehicle and 120 minutes, analogous to the three temporal clusters we

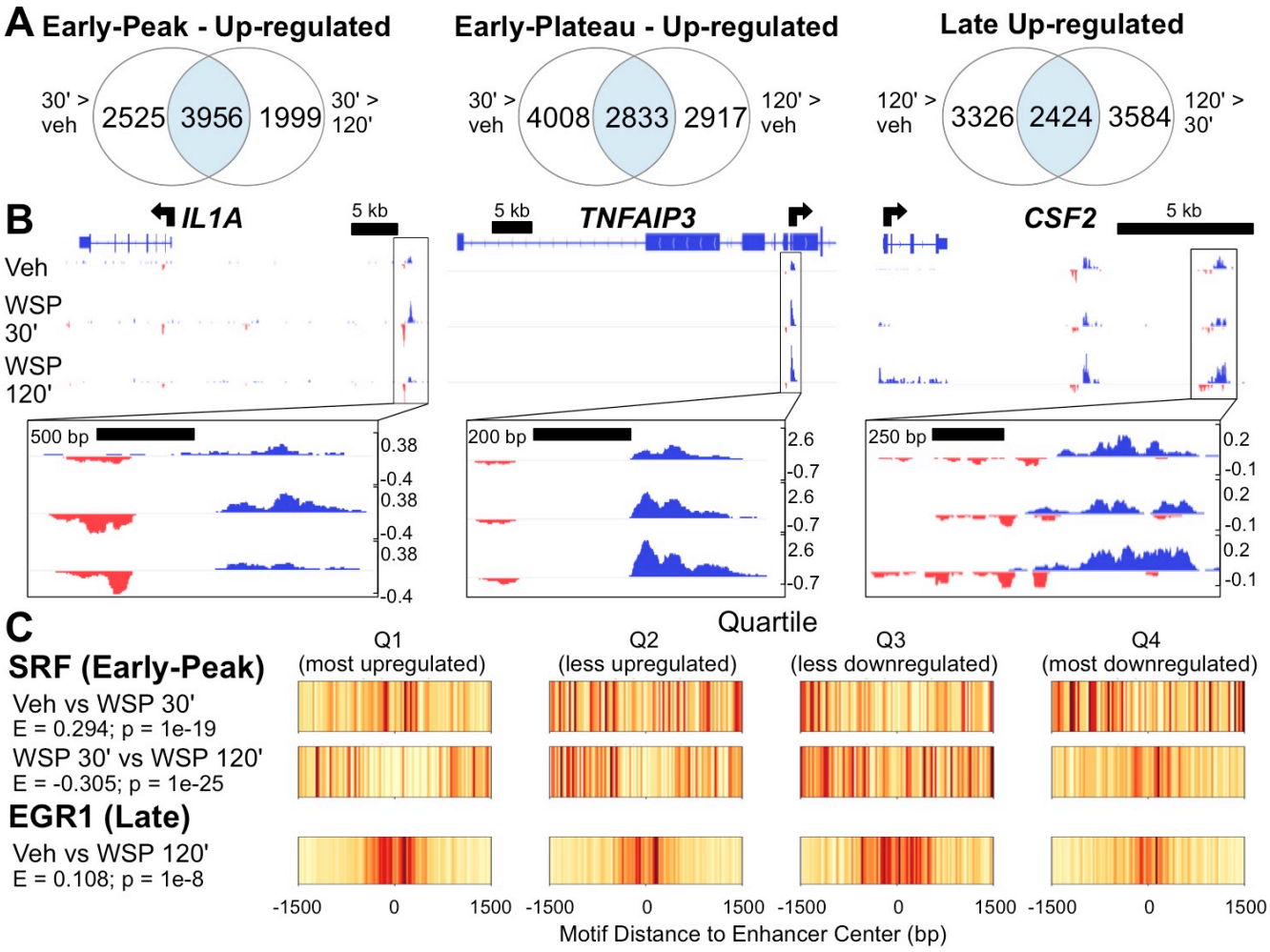

Figure 3. Genome-wide mapping of WSP-induced enhancer transcription defined by PRO-seq bidirectional signatures of RNA Polymerase II activity. (A) Venn diagrams indicating number of differentially regulated bidirectional transcripts (based on $p_{adj} < 0.05$) meeting indicated temporal clustering criteria, as described for Figure 2B. (B) IGV-visualized PRO-seq tracks of Tfit-called bidirectionals (boxed in black and magnified below each panel) and nearest genes exhibiting a similar pattern of regulation as representative examples of each temporal cluster characterized in (A). (C) Motif displacement distributions of significantly enriched transcription factor binding motifs within early-peak (top) versus late (bottom) clusters of differentially transcribed bidirectionals, as identified using TFEA. Each column represents the frequency of the indicated motif instance at the specified distance from the bidirectional center (labeled 0), where color specifies a normalized frequency relative to the entire 3kb region. Darker colors indicate greater enrichment on a 0-1 scale.

previously defined based on induction of transcription. Motifs for the TCF-SRF complex, which is activated in response to ERK and MAPK signaling (54,55), were identified as significantly enriched in the 30-minute data set in comparison to vehicle (e.g. Fig 3C, top), suggesting a rapid kinase-mediated transcriptional response to WSP. Comparison of 30 minutes to 120 minutes showed that enrichment of TCF and SRF motifs returned to baseline by 120 minutes, whereas EGR family motifs were enriched at 120 minutes in comparison to vehicle

(Figure 3C, bottom). These data suggest that dynamic changes in transcription factor utilization underlie different kinetics in transcriptional responses to WSP. Significantly enriched and depleted motifs for each treatment comparison are summarized in Supporting Table S13.

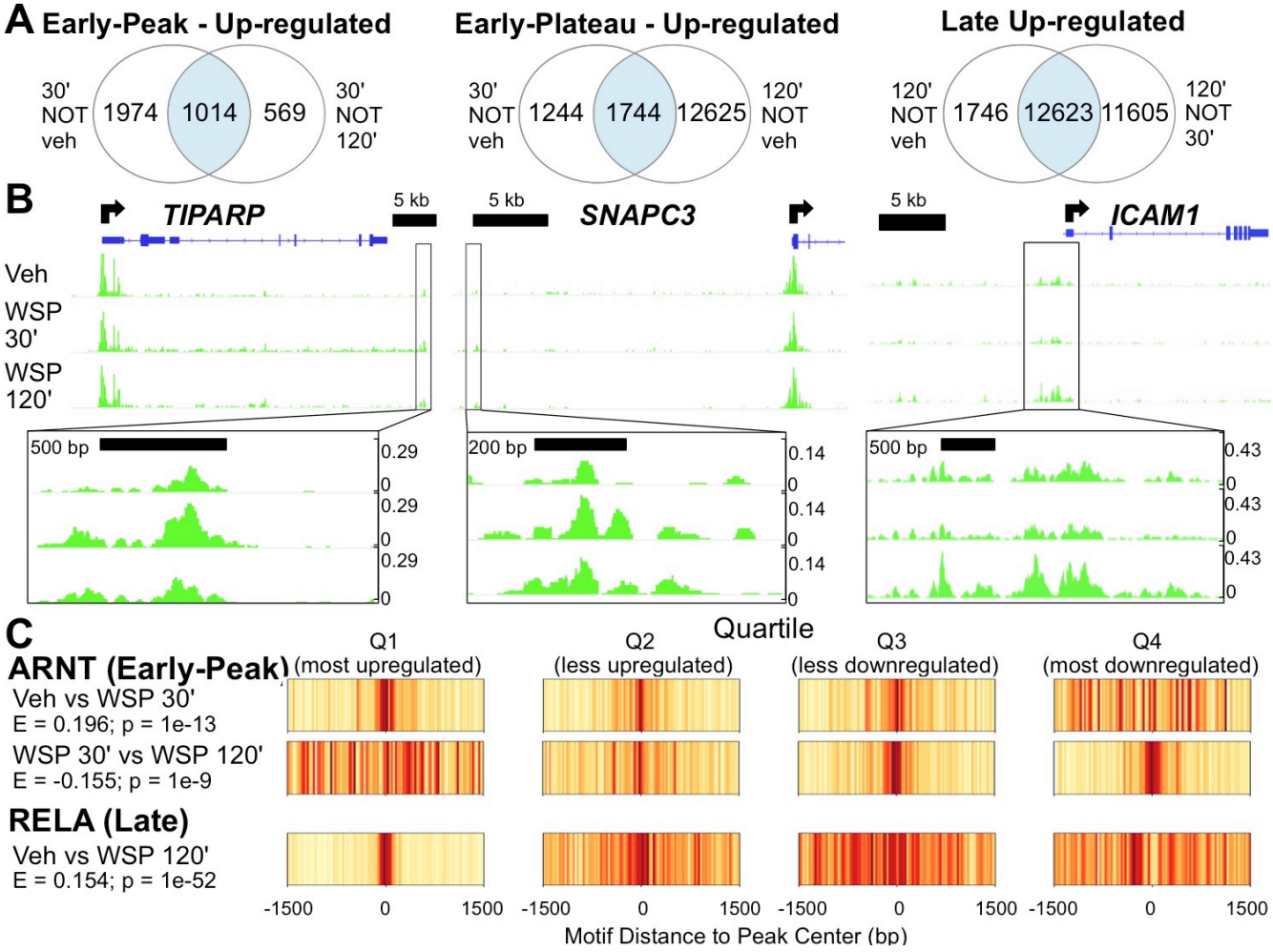

Figure 4. ATAC-seq demonstrates consistent temporal dynamics between chromatin accessibility and transcriptional responses to WSP and predicts key regulatory factors and pathways. (A) ATAC-seq was performed following exposure of Beas-2B cells to vehicle or WSP for 30 or 120 minutes. Venn diagrams indicate number of differentially regulated ATAC-seq peaks (based on $p_{adj} < 0.05$) meeting the indicated temporal clustering criteria, as described above. (B) IGV-visualized ATAC-seq tracks with MACS2-called peaks (boxed in black and magnified below each panel) and nearest genes exhibiting a similar pattern of regulation as representative examples of each temporal cluster characterized in (A). (C) Motif Displacement Distribution plots, as described for Figure 3C, from TFEA of differentially regulated MACS2-called ATAC-seq peaks representative of early-peak (top, ARNT) and late (RELA, bottom) differential motif enrichment.

Changes in chromatin structure identify AHR as driving early transcriptional responses to WSP

Some transcription factors are more associated with chromatin remodeling than directly altering RNA polymerase activity, and TFEA can also be applied to regions based on changes in chromatin structure to

identify these regulatory pathways (43). Therefore, to determine effects of WSP exposure on chromatin status, we performed the Assay for Transposase Accessible Chromatin using sequencing (ATAC-seq) in Beas-2B cells following 30 and 120 minutes of WSP exposure (42,56). Based on MACS2-defined peaks (57), we partitioned the ATAC-seq data temporally into the time-dependent clusters we had previously defined for nascent transcription (Figure 4A), noting that the number of new peaks occurring after 120 minutes of WSP was significantly greater than the number of new peaks at 30 minutes. Examples of loci that fall into each cluster are shown in Figure 4B. These data indicate that WSP causes significant chromatin remodeling, and the extent of chromatin remodeling in response to WSP increases over time.

As a further approach to define transcriptional mediators of genomic responses to WSP, we interrogated 3 kb regions centered on MACS2-defined ATAC-seq peaks using TFEA (58) to compare motif enrichment based on treatment and time. This analysis identified strong enrichment for the ARNT motif, the obligate AHR dimerization partner. This enrichment was evident at 30 minutes but decreased to baseline by 120 minutes (Figure 4C, top). In contrast, DME for RELA, a member of the NFkB complex, was significantly increased at 120 minutes but not 30 minutes (Figure 4C, bottom). These data strongly implicate AHR signaling as mediating early transcriptional responses to WSP in association with rapid chromatin remodeling, whereas effects of NFkB appear to peak at a later time.

Novel targets of AHR signaling defined through integrated genomics

In light of the known association of other forms of PM pollution with AHR signaling (25), and the identification of AHR through applying unbiased bioinformatics approaches to our genome-wide data, we scrutinized the early-peak cluster for canonical AHR target genes. We found a significant increase in transcription of numerous AHR targets at 30 minutes of WSP exposure that sharply decreased after 120 minutes (Table 1). Examples of integrated PRO-seq and ATAC-seq data for several established AHR targets, such as *CYP1B1,* and their associated enhancers visualized in IGV are shown in Figure 5A. Matinspector analysis of each of these dynamically regulated enhancer regions revealed matches for the canonical AHR/ARNT response element (59), implicating AHR as likely mediating these rapid transcriptional effects. In addition, we identified canonical

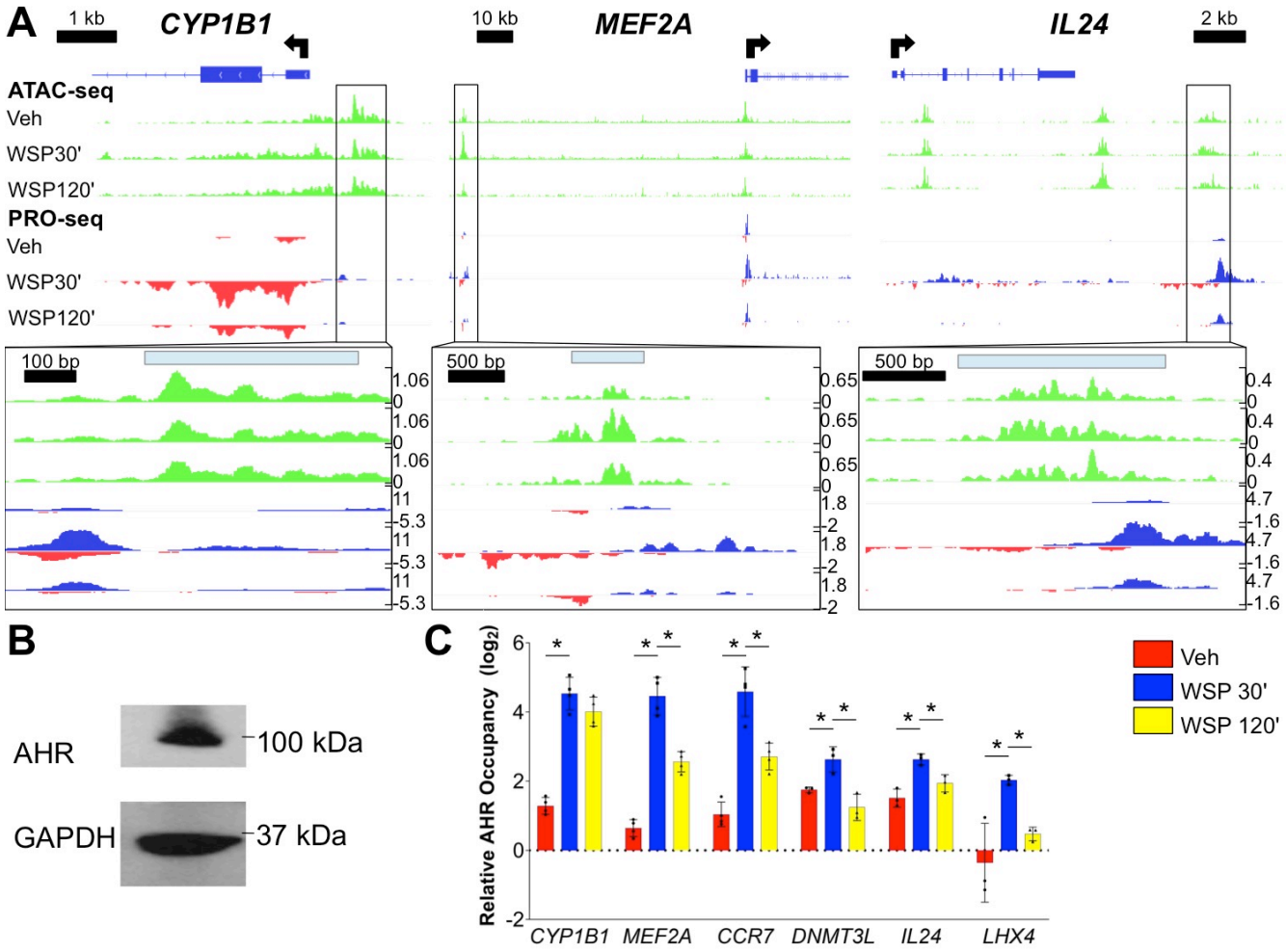

Figure 5. Integrated analysis of chromatin remodeling and nascent eRNA profiling datasets identifies sites of direct AHR occupancy and functional regulation of early-peak transcriptional targets of WSP. (A) ATAC-seq and PRO-seq tracks aligned in IGV at early-peak WSP response genes representing both canonical (*CYB1B1*, *MEF2A*) and novel (*IL24*) targets of AHR signaling. Associated early-peak eRNAs and ATAC-seq peaks are boxed and magnified below each panel, with locations of matches to the consensus AHR binding motif, determined using MatInspector, indicated by light blue bars. (B) Western blot verification of AHR protein expression in Beas-2B cells under basal culture conditions; GAPDH was a loading control. (C) qPCR primers were designed for the three regions described in (A) plus one other canonical (*CCR7*) and two additional novel (*DNMT3L*, *LHX4*) early-peak targets of AHR, then ChIP-qPCR was performed in Beas-2B cells following exposure to vehicle or WSP for 30 or 120 minutes. Bars represent AHR occupancy on a $\log_2$ scale (±SD), expressed as the mean C_T value at each target region relative to the geometric mean of C_T values at three negative control regions (n = 4/group, *$p < 0.05$ for indicated comparison).

AHR binding sites in regulatory regions for several other genes whose transcriptional responses to WSP were also consistent with the early peak response pattern. These presumptive AHR targets, many of which had not

Table 1: Canonical and novel putative AHR targets identified in the early-peak cluster of WSP-induced genes. P_{adj} values listed as 0 indicate infinitesimally small p_{adj} values that round to 0.

	Vehicle vs WSP 30 min		WSP 30 min vs WSP 120 min	
Gene	**Log_2 Fold Change**	**p_{adj}**	**Log_2 Fold Change**	**p_{adj}**
IL24	5.757	0	-2.359	6.81E-141
EGR1	5.491	0	-4.790	0
KRT17	5.128	0	-2.467	0
LHX4	5.066	0	-2.421	3.72E-152
MAFF	4.412	0	-2.869	0
TAGLN	4.169	0	-2.988	0
CCN2	3.798	0	-3.018	0
SPOCD1	3.629	0	-1.928	1.75E-158
TIPARP	2.777	0	-1.975	1.37E-282
SRF	2.773	0	-2.202	5.42E-218
MYH9	2.756	0	-1.797	6.60E-282
CYP1B1	2.508	0	-1.384	9.16E-126
DNMT3L	3.802	8.63E-280	-2.116	1.34E-116
AHRR	1.794	2.22E-238	-0.737	4.55E-41
CYP1A1	5.410	1.51E-224	-1.466	4.35E-45
ALDH3A1	2.512	2.58E-124	-0.992	1.21E-22
ARNT2	1.262	5.65E-72	-0.590	7.75E-17
MT2A	1.318	1.63E-64	-1.328	1.34E-64
MEF2A	0.836	4.16E-35	-0.994	6.95E-49
CCR7	2.153	1.43E-32	-1.560	1.24E-18
CYP1A2	4.662	7.97E-11	-2.324	9.82E-06

been previously linked to AHR signaling, are also listed in Table 1. Amongst these targets are *SPOCD1* and *DNMTL3*, which are reported to function within a protein complex to induce DNA methylation (60).

To definitively establish that AHR directs rapid and transient effects of WSP on airway epithelial gene expression, we performed ChIP-qPCR assays for AHR occupancy at several putative target loci. First, we confirmed by Western blot that AHR is expressed in this cell type (Figure 5B). Then we performed AHR ChIP-qPCR on Beas-2B cells following WSP exposure for 30 and 120 min. This demonstrated a gain in AHR occupancy in regulatory regions for canonical targets such as *CYP1A1*, as well as several novel targets, including *DNMT3L*, following exposure to WSP for 30 minutes (Figure 5C). AHR occupancy was decreased relative to the 30-minute time point after 120 minutes, consistent with the enhancer transcriptional signatures observed in the

PRO-seq datasets (Figures 5A). Thus, AHR directly and rapidly activates canonical target gene expression in response to WSP, however, AHR occupancy and direct effects on gene expression peak before 2 hours.

Crosstalk between AHR and NFkB signaling in response to WSP

Our data, in accordance with literature on other sources of PM pollution, suggest that both AHR and NFkB respond to WSP, but whether there is direct crosstalk between these pathways is unclear. To study the role of AHR in inflammatory transcriptional responses to WSP, we analyzed gene expression responses to WSP in the setting of siRNA-mediated knockdown of AHR or the RELA subunit of NFkB. Using qRT-PCR, we quantified the expression of several canonical AHR targets, as well as several established targets of NFkB (Figure 6A). After WSP exposure for 2 hours, *AHR* knockdown cells (verified by Western blotting, Figure 6B) demonstrated decreased expression of *AHRR* and *CYP1A1* in comparison to cells treated with si-Ctrl. There was no effect of

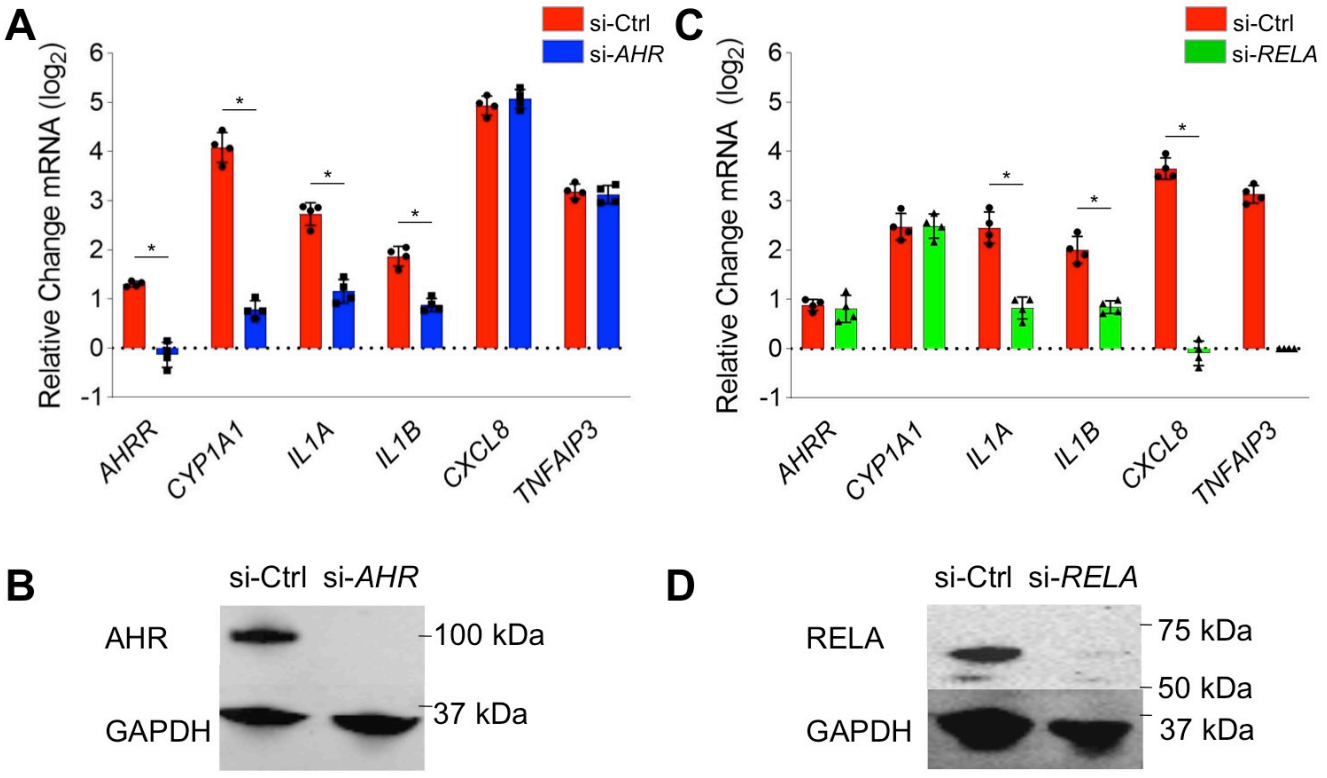

Figure 6. Airway epithelial inflammatory responses to WSP are mediated in part through complex crosstalk between AHR and NFKB. (A) Beas-2B cells transiently transfected with siRNA targeting AHR (si-*AHR*) or a scrambled control construct (si-Ctrl) were treated with vehicle or WSP for 2 hours and then assayed for indicated gene expression using qRT-PCR. Bars represent mean normalized C_T values on a $\log_2$ scale (±SD) relative to si-Ctrl+vehicle-treated controls (n = 4/group, *$p < 0.05$ for indicated comparison). (B) Western blot verification of AHR knockdown by si-*AHR* transfection. (C) si-*RELA*- or si-Ctrl-transfected Beas-2B cells were treated and assayed as described for (A). (D) Western blot verification of RELA knockdown by si-*RELA*.

AHR knockdown on expression of *CXCL8*, a prototypical NFkB target. Surprisingly, WSP-mediated increases in *IL1A* and *IL1B* expression were attenuated with AHR knockdown, indicating a direct or secondary role for AHR in inducing these cytokines in response to WSP. Knockdown of *RELA* resulted in an essentially reciprocal pattern, with a complete abrogation of *CXCL8* induction in response to WSP, a minimal effect on the induction of *AHRR* and *CYP1A1*, and an intermediate effect on *IL1A* and *IL1B* (Figures 6C-D). Thus, AHR and NFkB are both required for maximal increases in *IL1A* and *IL1B* expression in response to WSP, indicating functional crosstalk between AHR and inflammatory responses to WSP. Moreover, as *IL1A* and *IL1B* induce NFkB activity, these data indicate convergence of AHR and inflammatory signaling in a positive feedback circuit that may promote further inflammation.

Discussion

Transcriptional mechanisms underpinning effects of WSP on the airway epithelium, a topic of increasing importance given the expanding scope of wildfire pollution, had not been well defined. Through analyzing nascent transcription and performing ATAC-seq, here we show that airway epithelial cells undergo temporally dynamic changes in gene expression and chromatin structure in response to WSP, with transcriptional induction being the dominant effect after 30 minutes of exposure. We identified AHR as a likely early mediator of transcriptional responses to WSP using bioinformatics analysis, and we subsequently defined a set of canonical AHR targets that exhibit increased transcription after 30 minutes of WSP exposure in association with increased activity of nearby enhancers. Using ChIP, we established AHR occupancy at canonical XREs within enhancers and promoters for several target genes, and we further confirmed a role for AHR in mediating gene expression responses to WSP through knockdown experiments. WSP-induced expression of AHR target genes and associated enhancer activity returned to near baseline after 120 minutes of WSP exposure. In aggregate, our data establish a primary role for AHR in inducing transcriptional effects of WSP and define rapid kinetics of this AHR-mediated response.

PAHs found within various forms of air pollution are known to function as AHR ligands (61), however, direct induction of AHR by wood smoke particulates had not been previously reported. By virtue of the high resolution afforded by integrating PRO-seq and ATAC-seq data, we identified numerous canonical AHR target

genes that are rapidly induced in Beas-2B cells following WSP exposure, thereby expanding our understanding of AHR signaling with respect to air pollution in airway epithelial cells. We also defined a novel set of presumptive genes regulated by AHR based on rapid, transient transcriptional induction patterns and the discovery of enhancers for these genes harboring centrally located canonical XREs. Established and presumptive AHR target genes in Beas-2B cells (see Table 1) include genes encoding for proteins regulating cytoskeletal organization and cell junctions, such as *KRT17*, *TAGLN*, and *MYH9*, suggesting that barrier function of the airway epithelium is regulated by AHR signaling, as is already well-established for the gut and skin (62,63). Other rapidly induced targets included *CYP1A1* and *CYP1A2*, which metabolize AHR-activating PAHs that are found in WSP; the AHR repressor, *AHRR*; and *TIPARP*, an ADP-ribosyltransferase that represses AHR activity though ribosylation (64,65). Thus, in airway epithelial cells, at least three distinct negative feedback mechanisms regulated by AHR are implicated in the rapid decrease in transcription of primary AHR targets following WSP exposure.

In contrast to the powerful negative feedback system that limits the duration of direct effects of AHR on gene transcription, a number of genes we identified are candidates to mediate prolonged secondary responses to WSP-mediated activation of AHR signaling. For example, transcription of all three EGR transcription factors, *EGR1*, *EGR2* and *EGR3*, was induced after 30 minutes of WSP exposure. Based on TFEA indicating enrichment for motifs for each of these factors among active enhancers at 120 minutes versus vehicle (FDR < 0.05), our data implicate the EGR family in mediating secondary gene expression responses to WSP. In addition to this family, the bZip transcription factor, *MAFF*, and *LHX4*, a limb homeobox factor, were also rapidly induced by WSP. Canonical XREs within enhancers exhibiting increased activity in response to WSP were identified in proximity to each of these genes. Autocrine/paracrine regulators of airway cell programming, such as *CCN2* (CTGF), and the cytokine, *IL24*, which is implicated in lung and airway remodeling in response to different inflammatory stimuli, were also amongst the set of AHR targets we identified (66-69). Thus, the short-lived primary transcriptional response to WSP mediated by AHR includes targets that likely contribute to more sustained changes in gene expression. Although we observed induction of AHR targets in primary human small airway epithelial cells and similar kinetics, future work is needed to more fully establish the relevance and temporal

properties of AHR signaling responses to WSP in primary, differentiated airway epithelial cells cultured at air-liquid interface.

Persistent epigenetic changes such as DNA methylation, which can exert a memory effect on cell phenotype through modifying gene expression, are believed to contribute to long-term health effects of exposure to pollutants (70,71). Through PRO-seq, we identified rapid and transient induction in response to WSP of the DNA methylase, *DNMTL3*, and *SPOCD1*, which is implicated in recruiting *DNMTL3* to specific genomic loci in germline DNA (60). Although PAH-containing pollutants have been previously reported to cause increased DNA methylation (72,73), we are unaware of any reports that have identified specific methylation pathways that might mediate this epigenetic response to WSP or other pollutants containing AHR ligands. Whether this pathway is responsible for teratogenic and other long-term effects of AHR signaling, including altered DNA methylation, remains to be confirmed in future work.

In addition to AHR, we also identified NFkB as a mediator of transcriptional and chromatin responses to WSP in airway epithelial cells. Canonical targets of NFkB that were activated in response to WSP include *TNFAIP*3, *CXCL8*, and *IL1B*, among others. Knockdown of *RELA* confirmed that induction of *TNFAIP3* and *CXCL8* was largely dependent on the NFkB complex. Although other studies have implicated inflammasome activation in response to particulates as directly inducing NFkB activity (74), the mechanisms underlying NFkB activation in response to WSP remain to be elucidated. The timing of AHR and NFkB transcriptional motif utilization based on TFEA, however, suggests that NFkB-mediated responses to WSP occur in a temporally distinctive process from AHR signaling. Specifically, we observed significantly increased central NFkB motif enrichment within ATAC-seq peaks at the 120-minute time point relative to 30 minutes, whereas AHR motif utilization peaked at 30 minutes. Given the rapid induction of *IL1B* and *CXCL8* in response to WSP, both of which are known activators of NFkB signaling, NFkB activity in response to WSP exposure is likely partially attributable to positive feedback mediated through these and other cytokines that activate NFkB.

The physiologic consequences of AHR signaling as a response to PAHs and other exogenous ligands are controversial (32,75). Although the canonical model of AHR activation results in transcription of detoxifying Cytochrome P450 family enzymes, AHR is also involved in transcription of inflammatory target genes as we have observed here, and this latter process appears to persist beyond the detoxification response. Indeed,

inflammatory changes associated with environmental pollutants have implicated AHR as a key mediator in promoting the development of lung diseases such as asthma and COPD in various model systems (76). In contrast, alternative studies describe a protective role for AHR, such as a heightened inflammatory response in AHR knockout mice or AHR-mediated protection from apoptosis in cells exposed to cigarette smoke (76-78). To date, these differences have not been reconciled, although balance between canonical and non-canonical signaling, ligand-receptor interactions and pre-existing cellular states have been suggested as likely modifiers (32,36,75). In that regard, how specific PAH composition might influence these effects is not understood, and the mechanisms through which pulmonary diseases, such as COPD, interact with AHR-regulated pathways and potentially contribute to disease flares are unknown. These gaps in knowledge are of increasing importance given the growing seasonal intrusions of wildfire pollution into heavily populated areas in association with global warming (2,79,80). The primary transcriptional response to WSP and AHR signaling that we have defined here establishes a new framework for further investigations into the mechanisms underlying the health effects of wildfire smoke on the airway epithelium.

Acknowledgments. The CU Boulder BioFrontiers Sequencing facility provided invaluable technical assistance. **Funding:** This work was supported in part through NIH 2T32HL007085 (AG); NIH R01HL109557 (SKS, ANG); NIH R01GM125871 (MAG, LS, RDD). High Performance Computing resources (BioFrontiers Computing Core at CU Boulder) were funded by NIH 1S10OD012300.

References

1. Abatzoglou, J. T., and Williams, A. P. (2016) Impact of anthropogenic climate change on wildfire across western US forests. *Proceedings of the National Academy of Sciences* **113**, 11770-11775
2. Xu, R., Yu, P., Abramson, M. J., Johnston, F. H., Samet, J. M., Bell, M. L., Haines, A., Ebi, K. L., Li, S., and Guo, Y. (2020) Wildfires, Global Climate Change, and Human Health. *New England Journal of Medicine* **383**, 2173-2181
3. Reid, C. E., Brauer, M., Johnston, F. H., Jerrett, M., Balmes, J. R., and Elliott, C. T. (2016) Critical Review of Health Impacts of Wildfire Smoke Exposure. *Environmental health perspectives* **124**, 1334-1343
4. Adetona, O., Reinhardt, T. E., Domitrovich, J., Broyles, G., Adetona, A. M., Kleinman, M. T., Ottmar, R. D., and Naeher, L. P. (2016) Review of the health effects of wildland fire smoke on wildland firefighters and the public. *Inhal Toxicol* **28**, 95-139

5. Wu, C. M., Adetona, A., Song, C., Naeher, L., and Adetona, O. (2020) Measuring acute pulmonary responses to occupational wildland fire smoke exposure using exhaled breath condensate. *Archives of Environmental and Occupational Health* **75**, 65-69
6. Shin, S., Bai, L., Burnett, R. T., Kwong, J. C., Hystad, P., van Donkelaar, A., Lavigne, E., Weichenthal, S., Copes, R., Martin, R. V., Kopp, A., and Chen, H. (2020) Air Pollution as a Risk Factor for Incident COPD and Asthma: 15-Year Population-Based Cohort Study. *Am J Respir Crit Care Med*
7. Trieu, J., Yao, J., McLean, K. E., Stieb, D. M., and Henderson, S. B. (2020) Evaluating an Air Quality Health Index (AQHI) amendment for communities impacted by residential woodsmoke in British Columbia, Canada. *Journal of the Air & Waste Management Association (1995)* **70**, 1009-1021
8. Mirabelli, M. C., Ebelt, S., and Damon, S. A. (2020) Air Quality Index and air quality awareness among adults in the United States. *Environmental research* **183**, 109185
9. Cromar, K. R., Ghazipura, M., Gladson, L. A., and Perlmutt, L. (2020) Evaluating the U.S. Air Quality Index as a risk communication tool: Comparing associations of index values with respiratory morbidity among adults in California. *PLoS One* **15**, e0242031
10. Raun, L. H., Ensor, K. B., Pederson, J. E., Campos, L. A., and Persse, D. E. (2019) City-Specific Air Quality Warnings for Improved Asthma Self-Management. *American journal of preventive medicine* **57**, 165-171
11. Schweizer, D., Cisneros, R., Traina, S., Ghezzehei, T. A., and Shaw, G. (2017) Using National Ambient Air Quality Standards for fine particulate matter to assess regional wildland fire smoke and air quality management. *Journal of environmental management* **201**, 345-356
12. Tan, X., Han, L., Zhang, X., Zhou, W., Li, W., and Qian, Y. (2021) A review of current air quality indexes and improvements under the multi-contaminant air pollution exposure. *Journal of environmental management* **279**, 111681
13. Yao, J., Stieb, D. M., Taylor, E., and Henderson, S. B. (2020) Assessment of the Air Quality Health Index (AQHI) and four alternate AQHI-Plus amendments for wildfire seasons in British Columbia. *Canadian journal of public health = Revue canadienne de sante publique* **111**, 96-106
14. Ghio, A. J., Soukup, J. M., Dailey, L. A., Tong, H., Kesic, M. J., Budinger, G. R. S., and Mutlu, G. M. (2015) Wood Smoke Particle Sequesters Cell Iron to Impact a Biological Effect. *Chemical research in toxicology* **28**, 2104-2111
15. Dilger, M., Orasche, J., Zimmermann, R., Paur, H. R., Diabaté, S., and Weiss, C. (2016) Toxicity of wood smoke particles in human A549 lung epithelial cells: the role of PAHs, soot and zinc. *Archives of toxicology* **90**, 3029-3044
16. Arif, A. T., Maschowski, C., Garra, P., Garcia-Käufer, M., Petithory, T., Trouvé, G., Dieterlen, A., Mersch-Sundermann, V., Khanaqa, P., Nazarenko, I., Gminski, R., and Gieré, R. (2017) Cytotoxic and genotoxic responses of human lung cells to combustion smoke particles of Miscanthus straw, softwood and beech wood chips. *Atmospheric environment (Oxford, England : 1994)* **163**, 138-154

17. Rebuli, M. E., Speen, A. M., Martin, E. M., Addo, K. A., Pawlak, E. A., Glista-Baker, E., Robinette, C., Zhou, H., Noah, T. L., and Jaspers, I. (2019) Wood smoke exposure alters human inflammatory responses to viral infection in a sex-specific manner: A randomized, placebo-controlled study. *American Journal of Respiratory and Critical Care Medicine* **199**, 996-1007

18. Schwartz, C., Bølling, A. K., and Carlsten, C. (2020) Controlled human exposures to wood smoke: a synthesis of the evidence. *Particle and fibre toxicology* **17**, 49

19. Carlsten, C., MacNutt, M. J., Zhang, Z., Sava, F., and Pui, M. M. (2014) Anti-oxidant N-acetylcysteine diminishes diesel exhaust-induced increased airway responsiveness in person with airway hyper-reactivity. *Toxicological sciences : an official journal of the Society of Toxicology* **139**, 479-487

20. Kocbach, A., Herseth, J. I., Låg, M., Refsnes, M., and Schwarze, P. E. (2008) Particles from wood smoke and traffic induce differential pro-inflammatory response patterns in co-cultures. *Toxicology and applied pharmacology* **232**, 317-326

21. Danielsen, P. H., Møller, P., Jensen, K. A., Sharma, A. K., Wallin, H., Bossi, R., Autrup, H., Mølhave, L., Ravanat, J. L., Briedé, J. J., De Kok, T. M., and Loft, S. (2011) Oxidative stress, DNA damage, and inflammation induced by ambient air and wood smoke particulate matter in human A549 and THP-1 cell lines. *Chemical Research in Toxicology* **24**, 168-184

22. Vogel, C. F. A., Kado, S. Y., Kobayashi, R., Liu, X., Wong, P., Na, K., Durbin, T., Okamoto, R. A., and Kado, N. Y. (2019) Inflammatory marker and aryl hydrocarbon receptor-dependent responses in human macrophages exposed to emissions from biodiesel fuels. *Chemosphere* **220**, 993-1002

23. Traboulsi, H., Guerrina, N., Iu, M., Maysinger, D., Ariya, P., and Baglole, C. J. (2017) Inhaled Pollutants: The Molecular Scene behind Respiratory and Systemic Diseases Associated with Ultrafine Particulate Matter. *International journal of molecular sciences* **18**

24. Øvrevik, J., Refsnes, M., Låg, M., Holme, J. A., and Schwarze, P. E. (2015) Activation of Proinflammatory Responses in Cells of the Airway Mucosa by Particulate Matter: Oxidant- and Non-Oxidant-Mediated Triggering Mechanisms. *Biomolecules* **5**, 1399-1440

25. Weng, C. M., Wang, C. H., Lee, M. J., He, J. R., Huang, H. Y., Chao, M. W., Chung, K. F., and Kuo, H. P. (2018) Aryl hydrocarbon receptor activation by diesel exhaust particles mediates epithelium-derived cytokines expression in severe allergic asthma. *Allergy* **73**, 2192-2204

26. Provoost, S., Maes, T., Pauwels, N. S., Vanden Berghe, T., Vandenabeele, P., Lambrecht, B. N., Joos, G. F., and Tournoy, K. G. (2011) NLRP3/caspase-1-independent IL-1beta production mediates diesel exhaust particle-induced pulmonary inflammation. *J Immunol* **187**, 3331-3337

27. Tal, T. L., Simmons, S. O., Silbajoris, R., Dailey, L., Cho, S. H., Ramabhadran, R., Linak, W., Reed, W., Bromberg, P. A., and Samet, J. M. (2010) Differential transcriptional regulation of IL-8 expression by human airway epithelial cells exposed to diesel exhaust particles. *Toxicology and applied pharmacology* **243**, 46-54

28. Grilli, A., Bengalli, R., Longhin, E., Capasso, L., Proverbio, M. C., Forcato, M., Bicciato, S., Gualtieri, M., Battaglia, C., and Camatini, M. (2018) Transcriptional profiling of human bronchial epithelial cell BEAS-2B exposed to diesel and biomass ultrafine particles. *BMC Genomics* **19**, 302

29. Larigot, L., Juricek, L., Dairou, J., and Coumoul, X. (2018) AhR signaling pathways and regulatory functions. *Biochimie open* **7**, 1-9

30. Bock, K. W. (2020) Aryl hydrocarbon receptor (AHR)-mediated inflammation and resolution: Non-genomic and genomic signaling. *Biochem Pharmacol* **182**, 114220

31. Wilson, C. L., and Safe, S. (1998) Mechanisms of ligand-induced aryl hydrocarbon receptor-mediated biochemical and toxic responses. *Toxicologic pathology* **26**, 657-671

32. Rothhammer, V., and Quintana, F. J. (2019) The aryl hydrocarbon receptor: an environmental sensor integrating immune responses in health and disease. Nature Publishing Group

33. Haarmann-Stemmann, T., and Abel, J. (2006) The arylhydrocarbon receptor repressor (AhRR): structure, expression, and function. *Biol Chem* **387**, 1195-1199

34. Sakurai, S., Shimizu, T., and Ohto, U. (2017) The crystal structure of the AhRR-ARNT heterodimer reveals the structural basis of the repression of AhR-mediated transcription. *J Biol Chem* **292**, 17609-17616

35. Vondráček, J., Pěnčíková, K., Ciganek, M., Pivnička, J., Karasová, M., Hýžďalová, M., Strapáčová, S., Pálková, L., Neča, J., Matthews, J., Lom, M. V., Topinka, J., Milcová, A., and Machala, M. (2020) Environmental six-ring polycyclic aromatic hydrocarbons are potent inducers of the AhR-dependent signaling in human cells. *Environmental pollution (Barking, Essex : 1987)* **266**, 115125

36. Tian, J., Feng, Y., Fu, H., Xie, H. Q., Jiang, J. X., and Zhao, B. (2015) The Aryl Hydrocarbon Receptor: A Key Bridging Molecule of External and Internal Chemical Signals. *Environmental science & technology* **49**, 9518-9531

37. Bock, K. W. (2018) From TCDD-mediated toxicity to searches of physiologic AHR functions. *Biochem Pharmacol* **155**, 419-424

38. Julliard, W., Fechner, J. H., and Mezrich, J. D. (2014) The aryl hydrocarbon receptor meets immunology: friend or foe? A little of both. *Frontiers in immunology* **5**, 458

39. Sasse, S. K., Gruca, M., Allen, M. A., Kadiyala, V., Song, T., Gally, F., Gupta, A., Pufall, M. A., Dowell, R. D., and Gerber, A. N. (2019) Nascent transcript analysis of glucocorticoid crosstalk with TNF defines primary and cooperative inflammatory repression. *Genome Res* **29**, 1753-1765

40. Gally, F., Sasse, S. K., Kurche, J. S., Gruca, M. A., Cardwell, J. H., Okamoto, T., Chu, H. W., Hou, X., Poirion, O. B., Buchanan, J., Preissl, S., Ren, B., Colgan, S. P., Dowell, R. D., Yang, I. V., Schwartz, D. A., and Gerber, A. N. (2021) The MUC5B-associated variant rs35705950 resides within an enhancer subject to lineage- and disease-dependent epigenetic remodeling. *JCI insight* **6**

41. Huang da, W., Sherman, B. T., and Lempicki, R. A. (2009) Systematic and integrative analysis of large gene lists using DAVID bioinformatics resources. *Nat Protoc* **4**, 44-57

42. Corces, M. R., Trevino, A. E., Hamilton, E. G., Greenside, P. G., Sinnott-Armstrong, N. A., Vesuna, S., Satpathy, A. T., Rubin, A. J., Montine, K. S., Wu, B., Kathiria, A., Cho, S. W., Mumbach, M. R., Carter, A. C., Kasowski, M., Orloff, L. A., Risca, V. I., Kundaje, A., Khavari, P. A., Montine, T. J., Greenleaf, W. J., and Chang, H. Y. (2017) An improved ATAC-seq protocol reduces background and enables interrogation of frozen tissues. *Nat Methods* **14**, 959-962

43. Rubin, J. D., Stanley, J. T., Sigauke, R. F., Levandowski, C. B., Maas, Z. L., Westfall, J., Taatjes, D. J., and Dowell, R. D. (2020) Transcription factor enrichment analysis (TFEA): Quantifying the activity of hundreds of transcription factors from a single experiment. *bioRxiv*, 2020.2001.2025.919738

44. Grant, C. E., Bailey, T. L., and Noble, W. S. (2011) FIMO: scanning for occurrences of a given motif. *Bioinformatics* **27**, 1017-1018

45. Lambert, S. A., Jolma, A., Campitelli, L. F., Das, P. K., Yin, Y., Albu, M., Chen, X., Taipale, J., Hughes, T. R., and Weirauch, M. T. (2018) The Human Transcription Factors. *Cell* **175**, 598-599

46. Sasse, S. K., Mailloux, C. M., Barczak, A. J., Wang, Q., Altonsy, M. O., Jain, M. K., Haldar, S. M., and Gerber, A. N. (2013) The glucocorticoid receptor and KLF15 regulate gene expression dynamics and integrate signals through feed-forward circuitry. *Mol Cell Biol* **33**, 2104-2115

47. Altonsy, M. O., Sasse, S. K., Phang, T. L., and Gerber, A. N. (2014) Context-dependent cooperation between nuclear factor kappaB (NF-kappaB) and the glucocorticoid receptor at a TNFAIP3 intronic enhancer: a mechanism to maintain negative feedback control of inflammation. *J Biol Chem* **289**, 8231-8239

48. Park, E. J., and Park, K. (2009) Induction of pro-inflammatory signals by 1-nitropyrene in cultured BEAS-2B cells. *Toxicology letters* **184**, 126-133

49. Verstrepen, L., Carpentier, I., and Beyaert, R. (2014) The biology of A20-binding inhibitors of NF-kappaB activation (ABINs). *Adv Exp Med Biol* **809**, 13-31

50. Dukler, N., Booth, G. T., Huang, Y. F., Tippens, N., Waters, C. T., Danko, C. G., Lis, J. T., and Siepel, A. (2017) Nascent RNA sequencing reveals a dynamic global transcriptional response at genes and enhancers to the natural medicinal compound celastrol. *Genome Res* **27**, 1816-1829

51. Azofeifa, J. G., Allen, M. A., Hendrix, J. R., Read, T., Rubin, J. D., and Dowell, R. D. (2018) Enhancer RNA profiling predicts transcription factor activity. *Genome Res*

52. Azofeifa, J. G., and Dowell, R. D. (2017) A generative model for the behavior of RNA polymerase. *Bioinformatics* **33**, 227-234

53. Thorvaldsdóttir, H., Robinson, J. T., and Mesirov, J. P. (2012) Integrative Genomics Viewer (IGV): high-performance genomics data visualization and exploration. *Briefings in Bioinformatics* **14**, 178-192

54. Esnault, C., Gualdrini, F., Horswell, S., Kelly, G., Stewart, A., East, P., Matthews, N., and Treisman, R. (2017) ERK-Induced Activation of TCF Family of SRF Cofactors Initiates a Chromatin Modification Cascade Associated with Transcription. *Mol Cell* **65**, 1081-1095.e1085

55. Yates, P. R., Atherton, G. T., Deed, R. W., Norton, J. D., and Sharrocks, A. D. (1999) Id helix-loop-helix proteins inhibit nucleoprotein complex formation by the TCF ETS-domain transcription factors. *Embo j* **18**, 968-976

56. Buenrostro, J. D., Wu, B., Chang, H. Y., and Greenleaf, W. J. (2015) ATAC-seq: A Method for Assaying Chromatin Accessibility Genome-Wide. *Current protocols in molecular biology* **109**, 21.29.21-29

57. Feng, J., Liu, T., Qin, B., Zhang, Y., and Liu, X. S. (2012) Identifying ChIP-seq enrichment using MACS. *Nat Protoc* **7**, 1728-1740

58. Tripodi, I. J., Allen, M. A., and Dowell, R. D. (2018) Detecting Differential Transcription Factor Activity from ATAC-Seq Data. *Molecules (Basel, Switzerland)* **23**

59. Cartharius, K., Frech, K., Grote, K., Klocke, B., Haltmeier, M., Klingenhoff, A., Frisch, M., Bayerlein, M., and Werner, T. (2005) MatInspector and beyond: promoter analysis based on transcription factor binding sites. *Bioinformatics* **21**, 2933-2942

60. Zoch, A., Auchynnikava, T., Berrens, R. V., Kabayama, Y., Schöpp, T., Heep, M., Vasiliauskaitė, L., Pérez-Rico, Y. A., Cook, A. G., Shkumatava, A., Rappsilber, J., Allshire, R. C., and O'Carroll, D. (2020) SPOCD1 is an essential executor of piRNA-directed de novo DNA methylation. *Nature* **584**, 635-639

61. O'Driscoll, C. A., Gallo, M. E., Fechner, J. H., Schauer, J. J., and Mezrich, J. D. (2019) Real-world PM extracts differentially enhance Th17 differentiation and activate the aryl hydrocarbon receptor (AHR). *Toxicology* **414**, 14-26

62. Furue, M., Tsuji, G., Mitoma, C., Nakahara, T., Chiba, T., Morino-Koga, S., and Uchi, H. (2015) Gene regulation of filaggrin and other skin barrier proteins via aryl hydrocarbon receptor. *Journal of dermatological science* **80**, 83-88

63. Scott, S. A., Fu, J., and Chang, P. V. (2020) Microbial tryptophan metabolites regulate gut barrier function via the aryl hydrocarbon receptor. *Proceedings of the National Academy of Sciences of the United States of America* **117**, 19376-19387

64. Gomez, A., Bindesbøll, C., Satheesh, S. V., Grimaldi, G., Hutin, D., MacPherson, L., Ahmed, S., Tamblyn, L., Cho, T., Nebb, H. I., Moen, A., Anonsen, J. H., Grant, D. M., and Matthews, J. (2018) Characterization of TCDD-inducible poly-ADP-ribose polymerase (TIPARP/ARTD14) catalytic activity. *Biochem J* **475**, 3827-3846

65. MacPherson, L., Ahmed, S., Tamblyn, L., Krutmann, J., Förster, I., Weighardt, H., and Matthews, J. (2014) Aryl hydrocarbon receptor repressor and TiPARP (ARTD14) use similar, but also distinct mechanisms to repress aryl hydrocarbon receptor signaling. *International journal of molecular sciences* **15**, 7939-7957

66. Vu, Y. H., Hashimoto-Hachiya, A., Takemura, M., Yumine, A., Mitamura, Y., Nakahara, T., Furue, M., and Tsuji, G. (2020) IL-24 Negatively Regulates Keratinocyte Differentiation Induced by Tapinarof, an

Aryl Hydrocarbon Receptor Modulator: Implication in the Treatment of Atopic Dermatitis. *International journal of molecular sciences* **21**

67. Rao, L. Z., Wang, Y., Zhang, L., Wu, G., Zhang, L., Wang, F. X., Chen, L. M., Sun, F., Jia, S., Zhang, S., Yu, Q., Wei, J. H., Lei, H. R., Yuan, T., Li, J., Huang, X., Cheng, B., Zhao, J., Xu, Y., Mo, B. W., Wang, C. Y., and Zhang, H. (2020) IL-24 deficiency protects mice against bleomycin-induced pulmonary fibrosis by repressing IL-4-induced M2 program in macrophages. *Cell Death Differ*
68. Williams, A. E., Watt, J., Robertson, L. W., Gadupudi, G., Osborn, M. L., Soares, M. J., Iqbal, K., Pedersen, K. B., Shankar, K., Littleton, S., Maimone, C., Eti, N. A., Suva, L. J., and Ronis, M. J. J. (2020) Skeletal Toxicity of Coplanar Polychlorinated Biphenyl Congener 126 in the Rat Is Aryl Hydrocarbon Receptor Dependent. *Toxicological sciences : an official journal of the Society of Toxicology* **175**, 113-125
69. Wójcik-Pszczoła, K., Jakieła, B., Plutecka, H., Koczurkiewicz, P., Madeja, Z., Michalik, M., and Sanak, M. (2018) Connective tissue growth factor regulates transition of primary bronchial fibroblasts to myofibroblasts in asthmatic subjects. *Cytokine* **102**, 187-190
70. Eze, I. C., Jeong, A., Schaffner, E., Rezwan, F. I., Ghantous, A., Foraster, M., Vienneau, D., Kronenberg, F., Herceg, Z., Vineis, P., Brink, M., Wunderli, J. M., Schindler, C., Cajochen, C., Röösli, M., Holloway, J. W., Imboden, M., and Probst-Hensch, N. (2020) Genome-Wide DNA Methylation in Peripheral Blood and Long-Term Exposure to Source-Specific Transportation Noise and Air Pollution: The SAPALDIA Study. *Environmental health perspectives* **128**, 67003
71. Rider, C. F., and Carlsten, C. (2019) Air pollution and DNA methylation: effects of exposure in humans. *Clinical epigenetics* **11**, 131
72. Suhaimi, N. F., Jalaludin, J., and Abu Bakar, S. (2020) Deoxyribonucleic acid (DNA) methylation in children exposed to air pollution: a possible mechanism underlying respiratory health effects development. *Reviews on environmental health*
73. Martin, E. M., and Fry, R. C. (2018) Environmental Influences on the Epigenome: Exposure- Associated DNA Methylation in Human Populations. *Annual review of public health* **39**, 309-333
74. Kim, D. I., Song, M. K., and Lee, K. (2021) Diesel Exhaust Particulates Enhances Susceptibility of LPS-Induced Acute Lung Injury through Upregulation of the IL-17 Cytokine-Derived TGF-β(1)/Collagen I Expression and Activation of NLRP3 Inflammasome Signaling in Mice. *Biomolecules* **11**
75. Guarnieri, T., Abruzzo, P. M., and Bolotta, A. (2020) More than a cell biosensor: aryl hydrocarbon receptor at the intersection of physiology and inflammation. *American journal of physiology. Cell physiology* **318**, C1078-c1082
76. Thatcher, T. H., Maggirwar, S. B., Baglole, C. J., Lakatos, H. F., Gasiewicz, T. A., Phipps, R. P., and Sime, P. J. (2007) Aryl hydrocarbon receptor-deficient mice develop heightened inflammatory responses to cigarette smoke and endotoxin associated with rapid loss of the nuclear factor-kappaB component RelB. *The American journal of pathology* **170**, 855-864

77. Awji, E. G., Chand, H., Bruse, S., Smith, K. R., Colby, J. K., Mebratu, Y., Levy, B. D., and Tesfaigzi, Y. (2015) Wood smoke enhances cigarette smoke-induced inflammation by inducing the aryl hydrocarbon receptor repressor in airway epithelial cells. *American journal of respiratory cell and molecular biology* **52**, 377-386

78. Iu, M., Zago, M., Rico de Souza, A., Bouttier, M., Pareek, S., White, J. H., Hamid, Q., Eidelman, D. H., and Baglole, C. J. (2017) RelB attenuates cigarette smoke extract-induced apoptosis in association with transcriptional regulation of the aryl hydrocarbon receptor. *Free Radic Biol Med* **108**, 19-31

79. Cascio, W. E. (2018) Wildland fire smoke and human health. *The Science of the total environment* **624**, 586-595

80. (2018) Wildfire Trends in the United States — SciLine.

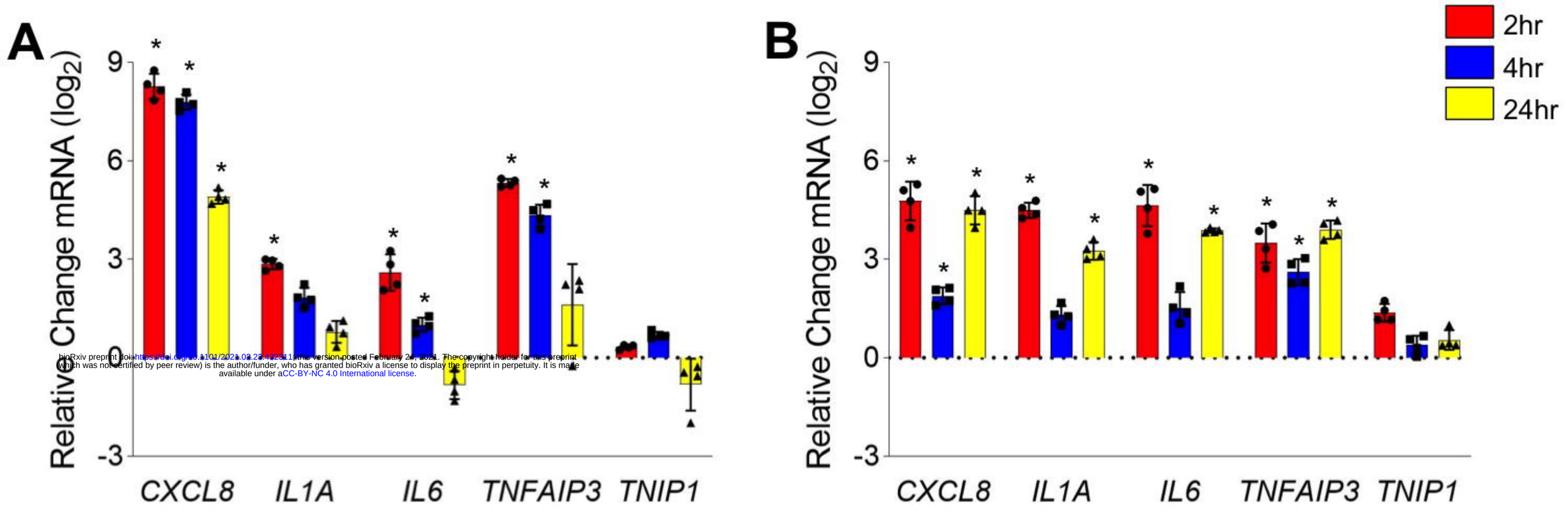

A

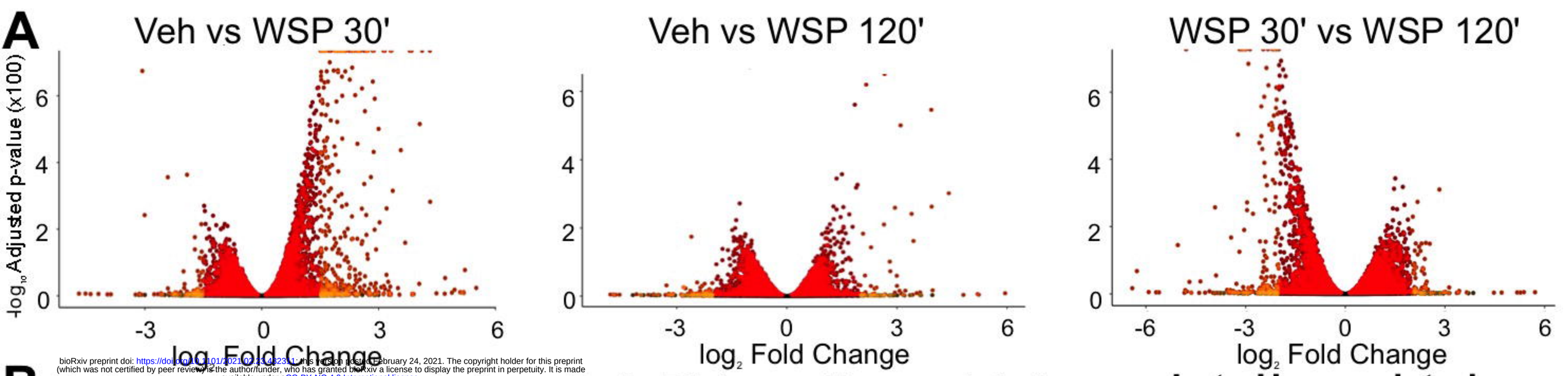

B

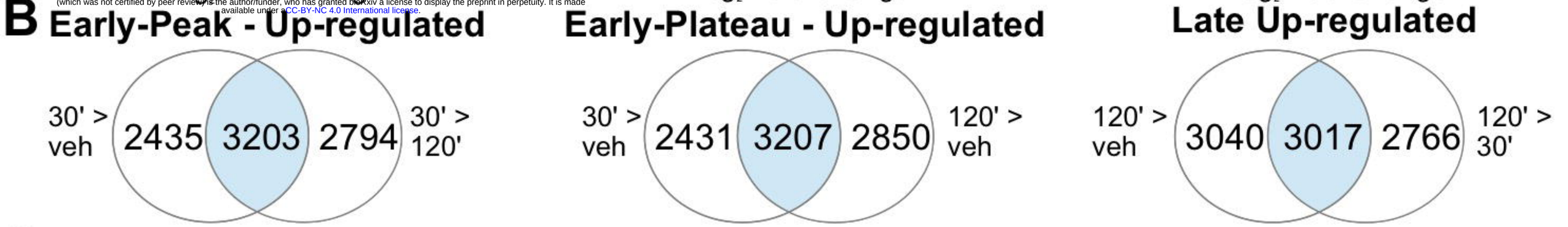

C

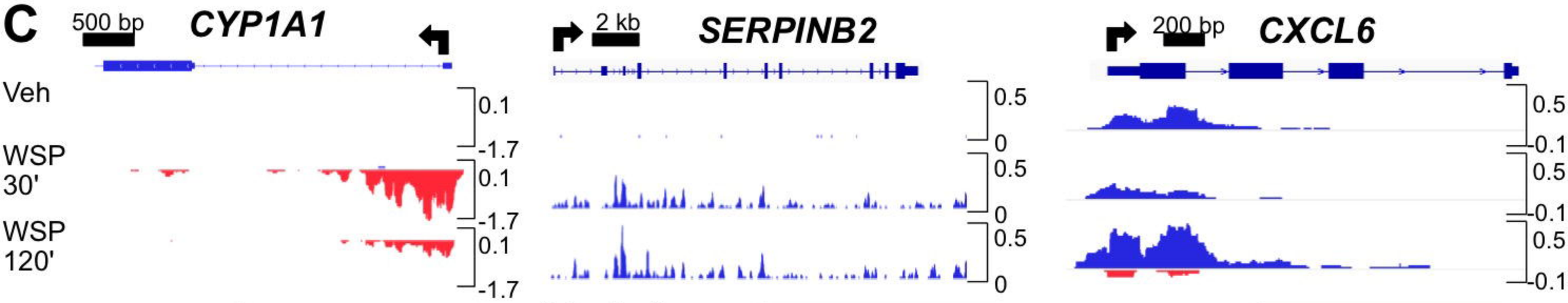

D